

# Direct Measurement of the Forbidden $2^3S_1 \rightarrow 3^3S_1$ Atomic Transition in Helium

K. F. Thomas, J. A. Ross, B. M. Henson, D. K. Shin, K. G. H. Baldwin, S. S. Hodgman, and A. G. Truscott  
*Laser Physics Centre, Research School of Physics,  
 The Australian National University,  
 Canberra, ACT 2601, Australia*  
 (Dated: December 1, 2023)

We present the detection of the highly forbidden  $2^3S_1 \rightarrow 3^3S_1$  atomic transition in helium, the weakest transition observed in any neutral atom. Our measurements of the transition frequency, upper state lifetime, and transition strength agree well with published theoretical values, and can lead to tests of both QED contributions and different QED frameworks. To measure such a weak transition, we developed two methods using ultracold metastable ( $2^3S_1$ ) helium atoms: low background direct detection of scattered atoms for sensitive measurement of the transition frequency and lifetime; and a pulsed atom laser heating measurement for determining the transition strength. These methods could be applied to other atoms, providing new tools in the search for ultra-weak transitions and precision metrology.

## Introduction

The field of precision spectroscopy has made many foundational contributions to modern physics [1–4], in particular through the development of quantum electrodynamics (QED) theory. However, despite QED being one of the most rigorously tested theories in physics, there are still elements within it that are poorly constrained, as shown by the recent measurements that required a re-assessment of the proton radius [5, 6]. This leads to an imperative to test QED at the highest precision using independent methods, in order to better understand its limitations.

Advances in laser technology have enabled the detection of an increasingly wide array of atomic transitions, including extremely weak atomic spectral lines from so-called forbidden transitions, which within a given approximation, e.g. the electric dipole approximation, strictly cannot occur. However, in reality such transitions do occur, but at extremely low rates. The strength of an atomic transition is characterized by the Einstein  $A$  coefficient (the transition rate), which is challenging to both calculate or measure accurately. However, in some atomic systems the Einstein  $A$  coefficient has a significant and potentially measurable contribution from QED effects [7]. Hence, measurements of the Einstein  $A$  coefficient can provide a test of QED, completely independent of, for example, the measurement of atomic energy intervals.

A favoured test bed of QED models is the helium atom, where the two-electron structure is simple enough that theoretical calculations of many parameters can be determined to great precision. For instance the  $2^3S_1 \rightarrow 2^1P_1$  transition (see Fig. 1), which is forbidden as it violates spin conservation and has a predicted Einstein  $A$  value of  $A = 1.4432 \text{ s}^{-1}$  [8], was first observed by Notermans *et al.* to precision of 0.5 MHz, thus providing a measurement of the  $2^1P_1$  lifetime [9]. Furthermore, a second extremely weak helium transition of interest is the singlet to

triplet ground state transition of metastable helium ( $\text{He}^*$ )  $2^3S_1 \rightarrow 2^1S_0$  (see Fig. 1), which is doubly forbidden, as it links a triplet to a singlet state, and  $\Delta l = 0$ . This transition has a predicted Einstein  $A$  coefficient ranging from  $A = 6.1 \times 10^{-8} \text{ s}^{-1}$  [10] to  $A = 1.5 \times 10^{-7} \text{ s}^{-1}$  [11], but the transition rate is yet to be measured. An experimental measurement of the transition frequency was carried out by van Rooij *et al.* to a precision of 2 kHz for both  $^3\text{He}$  and  $^4\text{He}$  [12], with subsequent measurements by Rengelink *et al.* improving the precision to 0.2 kHz by using a magic wavelength trap [13], providing a new test of QED and nuclear structure calculations.

Another transition in helium that until now has not been detected is the strongly forbidden  $2^3S_1 \rightarrow 3^3S_1$  transition (see Fig. 1), for which  $\Delta l = 0$ , and it is hence electric dipole forbidden. It is excited via the magnetic dipole interaction using light with a predicted wavelength of  $\sim 427.7 \text{ nm}$  [14]. There are unresolved conflicting theoretical predictions for the Einstein  $A$  coefficient of this transition. Derevianko *et al.* predict  $A = 1.17 \times 10^{-8} \text{ s}^{-1}$  [15], while a calculation by Lach *et al.* gives  $A = 6.48 \times 10^{-9} \text{ s}^{-1}$  [16], which states in reference to the differing values “*This discrepancy does not have experimental impact since this rate is too small ... to be measured*” [16]. An accurate measurement of the Einstein  $A$  coefficient for this transition would provide insight into the validity and limitations of the different approaches within QED theory. These calculations also indicate that this transition rate would be the weakest ever measured in a neutral atom, and only slightly stronger than the weakest measured transition rate in an ion: the electric-octupole transition in  $^{172}\text{Yb}^+$  which is the longest lived at 8.4 years, *i.e.*  $A = 3.8 \times 10^{-9} \text{ s}^{-1}$  (theory [17]), or  $10_{-4}^{+7}$  years, equivalently  $A = 3_{-1}^{+2} \times 10^{-9} \text{ s}^{-1}$  (experiment [18]).

In this work we present the first detection of the  $2^3S_1 \rightarrow 3^3S_1$  transition in  $^4\text{He}$ . We develop two novel techniques for the measurement of ultra-weak transitions and use them to determine the transition frequency, Einstein  $A$  coefficient and excited state lifetime. The first

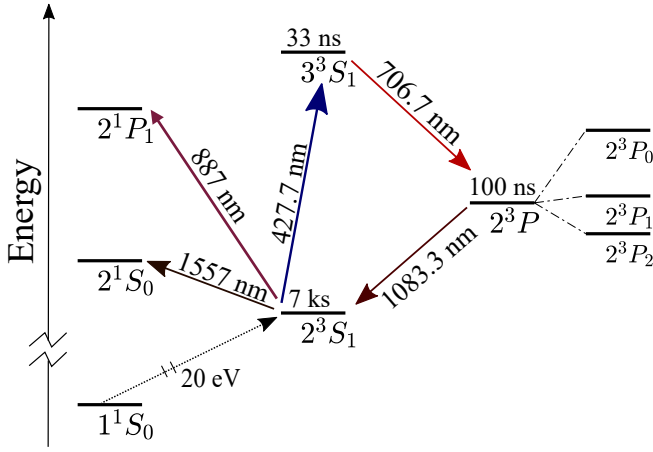


FIG. 1. Partial atomic level scheme for helium. Level splittings are not to scale. The transition of interest,  $2^3S_1 \rightarrow 3^3S_1$ , is 427.7 nm (blue arrow), along with the dominant decay path from the  $3^3S_1$  state (706.7 nm, red arrow). Relevant excited state lifetimes and transition wavelengths are also indicated.

method uses a Bose-Einstein condensate (BEC) and directly detects atoms which absorb a photon and escape a shallow trap. While this method is highly sensitive and is ideal for the determination of the transition frequency and linewidth, the uncertainty in the collection efficiency necessitates an independent approach for determining the Einstein  $A$  coefficient. To this end we developed a second method, which measures the heating rate of a trapped thermal cloud due to scattered photons from a probe beam by repeatedly measuring the temperature with a pulsed outcoupling scheme. From this the Einstein  $A$  coefficient can be extracted. These techniques could be used to search for other weak transitions which have applications in astronomy and new technologies, such as atomic clocks.

### Direct Detection of the Transition Frequency

To measure the transition frequency and linewidth we start with a BEC of  $\sim 10^6$  metastable helium ( $\text{He}^*$ ) atoms trapped in the long-lived  $2^3S_1$  excited state [19], prepared via a combination of laser and evaporative cooling in a magnetic bi-planar quadrupole Ioffe trap [20]. The atoms are detected after falling onto an 80 mm diameter micro-channel plate and delay line detector (DLD) [21], located approximately 850 mm below the trap centre (Fig. 2).

To address the  $2^3S_1 \rightarrow 3^3S_1$  transition we illuminate the atoms with a probe beam from a laser and doubling cavity that is tuneable around 427.7 nm [22]. The frequency of the laser was stabilised using a feedback loop to a wavemeter with 2 MHz absolute accuracy, which was periodically calibrated to a known cesium crossover transition (see [22] for further detail). After passing through

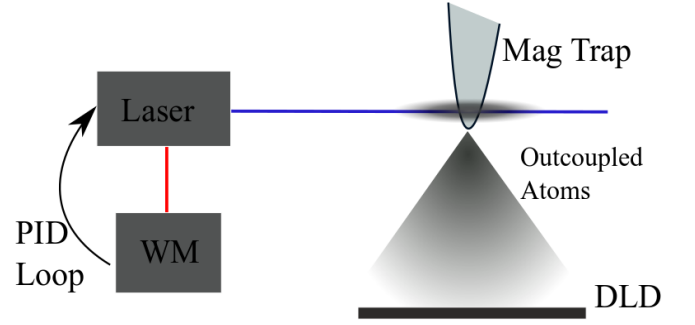


FIG. 2. Diagram of the experimental setup. A BEC is produced and then held in a magnetic trap. The laser light is focused onto the atoms in the trap and when an atom absorbs one of the photons it will most likely leave the trap, with some high probability of it landing on the detector.

an optical fibre, the probe beam is focused and aligned along the weak axis of the trap, see Fig. 2 for diagram of experimental setup. We then perform differential measurements between the laser applied and a reference shot with the laser blocked.

The transition is detected by directly measuring small numbers of atoms that absorb the probe laser light, during a 25 s exposure time. When the wavelength of a  $\sigma^-$  polarised probe laser beam is resonant with the  $2^3S_1 \rightarrow 3^3S_1$  transition, the 427.7 nm photon excites the atom from the  $2^3S_1, m_J = +1$  state to the  $3^3S_1, m_J = 0$  state and the atom receives a momentum recoil. The vast majority of these excited atoms then decay within  $\sim 30$  ns, emitting a photon at 706.7 nm to one of the  $2^3P_{0,1,2}$  states, then within  $\sim 100$  ns decay via the 1083 nm transitions to the  $2^3S_1$  state (see Fig. 1). This is because all other transitions from  $3^3S_1$  and the  $2^3P_{0,1,2}$  states are forbidden: hence less than 1 in  $10^4$  atoms will decay to non- $2^3S_1$  states [23, 24].

Atoms will hence on average end up distributed among the magnetic sublevels  $m_J = (-1, 0, 1)$  of the  $2^3S_1$  state with a fractional population of (24%, 52%, 24%) based on the relevant transition Clebsch-Gordan coefficients. The 76% of atoms that decay to the untrapped  $2^3S_1, m_J = 0$  or  $-1$  states leave the trap immediately and fall under the influence of gravity onto the DLD, with the chance that they will scatter off other atoms while leaving the BEC [22].

The remaining 24% of scattered atoms in the  $2^3S_1, m_J = +1$  state will be re-trapped.

After the probe beam is switched off, the remaining un-scattered atoms in the magnetic trap are outcoupled with pulses of broadband RF radiation. This transfers all atoms from the trap into an atom laser [21, 25], allowing the total number of un-scattered atoms in the trap to be measured, while avoiding detector saturation. The ratio of scattered to unscattered atoms can hence be determined, which is less sensitive to total BEC number

fluctuations from shot-to-shot.

For each laser wavelength,  $\sim 215$  shots are taken with the probe beam applied and  $\sim 50$  with it blocked as a reference, from which the normalised scattering probability per photon per unit time [22] is extracted. The scattered fractions for a range of frequencies around the transition are shown in Fig. 3. At resonance, we measure a peak signal corresponding to 0.34% of the total atoms scattered per  $\sim 10^{18}$  (or 0.65 J) applied photons. Note that the signal in Fig. 3 decays to a negative value far from the transition. We speculate that this is due to the off-resonant repulsive dipole potential of the probe beam on the atoms, which causes a deflection of atoms such that they miss the detector, compared to the reference case.

The centre of the corresponding Lorentzian fit gives a measured transition frequency of  $f_{0,d} = 700,939,271.64(8)$  MHz, with subscript  $d$  referring to the direct detection method and with only the statistical uncertainty shown. After applying relevant systematic corrections (as listed with the full error budget in Tab. I), this yields a final value of  $f_{0,d}^{shifted} = 700,939,271(5)$  MHz. This agrees extremely well with the most recent published value in the literature of 700,939,269(8) MHz [14], with our uncertainty smaller than that of theory. The Lorentzian width of the peak also allows the excited state lifetime of the  $3^3S_1$  state to be determined, once external systematic effects such as laser power broadening are removed [22]. We estimate an excited state lifetime of  $\tau = 33(6)$  ns, which compares

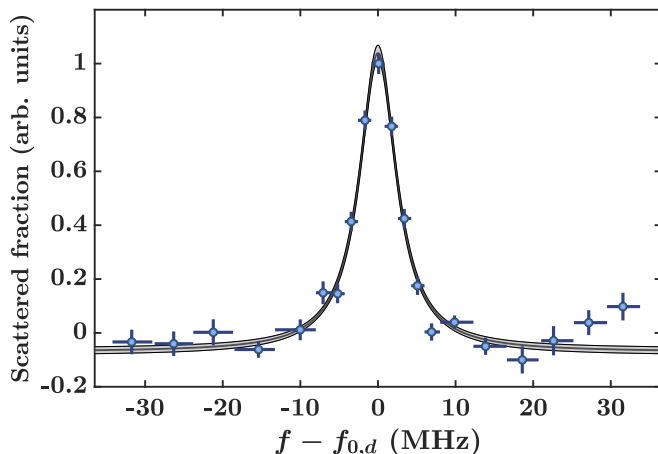


FIG. 3. (Color online) The normalised scattered fraction as a function of applied laser frequency (relative to the fitted centered frequency  $f_{0,d} = 700,939,271.64(8)$  MHz). Data has been binned for viewing, with vertical bars indicating standard error and horizontal bars indicating the limits of the bin. The black line is a Lorentzian fit to the data, with the grey shaded region indicating the confidence interval. The full width at half maximum of the fit is 5.7(3) MHz, corresponding to an excited state lifetime of 33(6) ns. The peak signal represents a scattered fraction of 0.34% for a time integrated power of 0.65 J.

well to the theoretical value of 35.9(2) ns [22].

### Heating Detection for Measurement of Transition Strength

To measure the transition strength, we employ a different experimental technique that determines the heating of the cloud induced by scattered photons from the probe beam. The thermal cloud has an initial temperature of order 1  $\mu$ K. By outcoupling atoms using a single minimally-destructive, sufficiently Fourier-broadened RF pulse that uniformly removes  $\sim 2\%$  of the atoms, the time-of-flight profile recorded on the DLD in the far field will represent the momentum profile of the trapped atoms [26]. As the temperature of the atoms is significantly above the condensation temperature,  $T_c \sim 150$  nK, this profile is well approximated by a Boltzmann distribution. Hence a Gaussian fit to a single outcoupled pulse of atoms provides a temperature measurement of the cloud at that point in time.

By repeatedly outcoupling small numbers of atoms (the full sequence uses 95 pulses each spaced 240 ms apart), the temperature of the trapped thermal cloud can be estimated as a function of time, and thus a heating rate determined. Comparison of the measured heating rate when the probe beam is present to when it is blocked allows an estimate of the heating rate due to the probe beam. The difference in the heating rates between probe and reference is shown in Fig. 4 as a function of laser frequency, which gives a fitted peak frequency for this method of  $f_{0,h}^{shifted} = 700,939,270.9(6)$  MHz, (with subscript  $h$  referring to the heating method, and with the statistical uncertainty shown). After applying appropriate systematic frequency shifts (see Tab. I [22]), the final value for the transition frequency is  $f_{0,h} =$

Value	Systematic Freq Shift (MHz)		Unc (MHz)	
	$f_{0,d}$	$f_{0,h}$	$f_{0,d}$	$f_{0,h}$
Zeeman shift	-1.715		0.003	
AC Stark shift	6.9	5.9	1.5	1.6
DC Stark shift	$< 10^{-6}$		-	
Mean field shift	$< 0.01$		-	
Recoil shift	0.273		$< 0.001$	
Cesium Cell offset				
- AC Stark shift	-1.9		0.4	
- Vapour shift	$< 0.006$		-	
Wavemeter	-3.0		4.1	
Statistical	-		0.08	0.6
Total	0.6	-0.4	4.4	4.5

TABLE I. Systematic shifts, corrections, and uncertainties to measured frequency values from the direct detection method  $f_{0,d}$  and the heating method  $f_{0,h}$ . Note that uncertainties are added in quadrature.

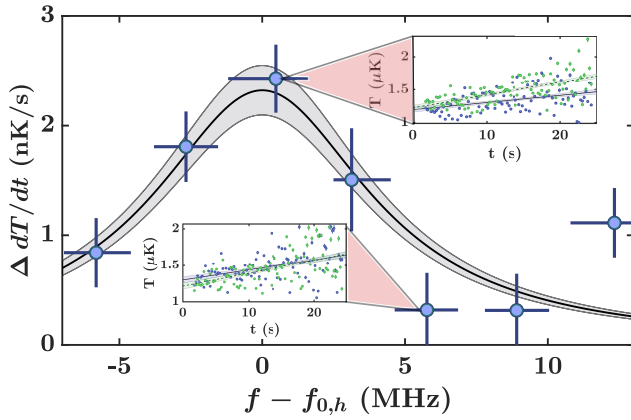


FIG. 4. (Color online) Increase in heating rate as a function of applied laser frequency, relative to fitted rate frequency center  $f_{0,h} = 700,939,270.9(6)$  MHz. Data has been binned in frequency for clarity, with error bars indicating bin width and standard deviation. The insets show a comparison of heating rates at the respective frequencies, with the dashed (green) line indicating a run with the laser light applied and the solid (blue) line indicating a reference run.

700,939,271(5) MHz, and the excited state lifetime is 40(20) ns. Both agree within uncertainty with the values measured by the direct detection method.

Furthermore, the measured heating rate combined with the heat capacity of the atomic cloud allows us to calculate the Einstein  $A$  coefficient [22]. The resultant value is  $A = 7(4) \times 10^{-9} \text{ s}^{-1}$ , compared to the most recent theoretical value of  $A = 6.48 \times 10^{-9} \text{ s}^{-1}$  [16]. For reference we find the weakest transitions the heating method could ideally detect, based upon the statistical uncertainty in the data and for our experimental conditions, to be  $A_{\min} \sim 1.8 \times 10^{-9} \text{ s}^{-1}$  [22]. The absolute value of this fundamental limiting sensitivity is far below that of other techniques, which historically have had similar relative uncertainties of 25% to 50% but absolute uncertainties of  $\sim 10^3 \text{ s}^{-1}$  [27, 28].

Method	Center Freq (MHz)	$3^3S_1$ State Lifetime (ns)	Einstein $A$ Coeff ( $10^{-9}\text{s}^{-1}$ )
Direct	700,939,271(5)	33(6)	-
Heating	700,939,271(5)	40(20)	7(4)
Theory	700,939,269(8)[14]	35.9(2)[22]	6.48[16], 11.7[15]

TABLE II. Summary table of experimentally measured values, including all systematic corrections, for the  $2^3S_1 \rightarrow 3^3S_1$  transition in Helium, with the most recent theoretical calculations for comparison.

## Discussion and Conclusion

Our results for the transition frequency using both methods compare well with the most recent theoretical value in the literature (see Tab. II), and our experimental uncertainty is comparable to that of the current QED theory calculation. Furthermore, a consequence of our measurement of the  $2^3S_1 \rightarrow 3^3S_1$  transition wavelength is that it constrains the  $2^3P_1 \rightarrow 3^3S_1$  transition frequency to be 424,202,774(5) MHz, using the extremely accurately measured  $2^3S_1 \rightarrow 2^3P_1$  transition frequency [29]. Further, the experimental Einstein  $A$  coefficient also agrees within error with both of the most recent theoretical published values [15, 16], although it is not sufficiently sensitive to resolve the difference between them. However, our limiting sensitivity is far below the discrepancy between the two ( $1.8 \times 10^{-9} \text{ s}^{-1}$  compared to  $5.2 \times 10^{-9} \text{ s}^{-1}$ ), thus further measurements could resolve the two providing insight into the validity of the conflicting approaches used to calculate the theoretical values.

In conclusion, we have demonstrated a new extremely sensitive method for measuring and characterising spectroscopic transitions. This has allowed us to detect the weakest transition ever observed in a neutral atom. The techniques are based upon momentum detection of atoms, separating them from most other techniques in the literature which are usually based upon measuring change in irradiance. While our method agrees within experimental uncertainty with theory, by increasing the accuracy of the laser wavelength measurement (e.g. via incorporating a frequency comb), we could reach a level of accuracy of  $< 1$  MHz, which would provide a challenge to improve state-of-the-art theoretical predictions. Furthermore, by conducting similar measurements on  $^3\text{He}$ , isotope shifts could also be compared as a further test of QED predictions.

We have also found that the limiting sensitivity of our techniques is far below that of other such techniques used to measure Einstein  $A$  coefficients [27]. The high sensitivity of our technique for extremely weak transitions in principle could be extended to measure weak transitions in other atoms, which are important in precision metrology and astronomy [28]. A key application of weak transitions is to atomic clocks, and our techniques could be extended to search for new clock transitions, such as the nuclear clock transition in thorium [30–33].

The authors would like to thank G. W. F. Drake, G. Lach and K. Pachucki for helpful discussions, and C. J. Vale and S. Hoinka for the loan of the laser. This work was supported through Australian Research Council (ARC) Discovery Project Grants DP160102337 and DP180101093, as well as Linkage Project LE180100142.

K.F.T. and D.K.S. are supported by Australian Government Research Training Program (RTP) Scholarships. S. S. H. is supported by ARC Discovery Early Career Researcher Award No. DE150100315.

- 
- [1] A. H. Compton, A quantum theory of the scattering of X-rays by light elements, *Phys. Rev.* **21**, 483 (1923).
  - [2] G. Landsberg and L. Mandelstam, A novel effect of light scattering in crystals, *Naturwissenschaften* **16**, 557 (1928).
  - [3] C. V. Raman and K. S. Krishnan, The optical analogue of the Compton effect, *Nature* **121**, 711 (1928).
  - [4] W. E. Lamb and R. C. Retherford, Fine structure of the hydrogen atom by a microwave method, *Phys. Rev.* **72**, 241 (1947).
  - [5] N. Bezginov, T. Valdez, M. Horbatsch, A. Marsman, A. C. Vutha, and E. A. Hessels, A measurement of the atomic hydrogen lamb shift and the proton charge radius, *Science* **365**, 1007 (2019).
  - [6] W. Xiong, A. Gasparian, H. Gao, *et al.*, A small proton charge radius from an electron-proton scattering experiment, *Nature* **575**, 147 (2019).
  - [7] O. Y. Andreev, L. N. Labzowsky, and G. Plunien, Qed calculation of transition probabilities in two-electron ions, *Phys. Rev. A* **79**, 032515 (2009).
  - [8] G. W. F. Drake and D. C. Morton, A multiplet table for neutral helium (4heI) with transition rates, *The Astrophysical Journal Supplement Series* **170**, 251 (2007).
  - [9] R. P. M. J. W. Notermans and W. Vassen, High-precision spectroscopy of the forbidden  $2^3S_1 \rightarrow 2^1P_1$  transition in quantum degenerate metastable helium, *Phys. Rev. Lett.* **112**, 253002 (2014).
  - [10] E. V. Baklanov and A. V. Denisov, Probability of the  $2^1S_0 - 2^3S_1$  forbidden transition in the helium atom, *Quantum Electronics* **27**, 463 (1997).
  - [11] C. D. Lin, W. R. Johnson, and A. Dalgarno, Radiative decays of the  $n = 2$  states of he-like ions, *Phys. Rev. A* **15**, 154 (1977).
  - [12] R. van Rooij, J. S. Borbely, J. Simonet, M. D. Hoogerland, K. S. E. Eikema, R. A. Rozendaal, and W. Vassen, Frequency metrology in quantum degenerate helium: Direct measurement of the  $2^3S_1 \rightarrow 2^1S_0$  transition, *Science* **333**, 196 (2011).
  - [13] R. J. Rengelink, Y. van der Werf, R. P. M. J. W. Notermans, R. Jannin, K. S. E. Eikema, M. D. Hoogerland, and W. Vassen, Precision spectroscopy of helium in a magic wavelength optical dipole trap, *Nature Physics* **14**, 1132 (2018).
  - [14] G. W. F. Drake, *Springer handbook of atomic, molecular, and optical physics* (2006) Chap. High Precision Calculations for Helium, pp. 199–219.
  - [15] A. Derevianko, I. M. Savukov, W. R. Johnson, and D. R. Plante, Negative-energy contributions to transition amplitudes in heliumlike ions, *Phys. Rev. A* **58**, 4453 (1998).
  - [16] G. Lach and K. Pachucki, Forbidden transitions in the helium atom, *Phys. Rev. A* **64**, 042510 (2001).
  - [17] E. Biémont and P. Quinet, Theoretical study of the  $4f^{14}6s\ 2S_{1/2} - 4f^{13}6s^2\ 2F_{7/2}^0\ E3$  transition in Yb II, *Phys. Rev. Lett.* **81**, 3345 (1998).
  - [18] M. Roberts, P. Taylor, G. P. Barwood, P. Gill, H. A. Klein, and W. R. C. Rowley, Observation of an electric octupole transition in a single ion, *Phys. Rev. Lett.* **78**, 1876 (1997).
  - [19] S. S. Hodgman, R. G. Dall, L. J. Byron, K. G. H. Baldwin, S. J. Buckman, and A. G. Truscott, Metastable helium: A new determination of the longest atomic excited-state lifetime, *Phys. Rev. Lett.* **103**, 053002 (2009).
  - [20] R. Dall and A. Truscott, Bose-Einstein condensation of metastable helium in a bi-planar quadrupole Ioffe configuration trap, *Optics Communications* **270**, 255 (2007).
  - [21] A. G. Manning, S. S. Hodgman, R. G. Dall, M. T. Johnson, and A. G. Truscott, The Hanbury Brown-Twiss effect in a pulsed atom laser, *Opt. Express* **18**, 18712 (2010).
  - [22] See Supplementary Material for details.
  - [23] R. G. Dall, K. G. H. Baldwin, L. J. Byron, and A. G. Truscott, Experimental determination of the helium  $2^3P_1 - 1^1S_0$  transition rate, *Phys. Rev. Lett.* **100**, 023001 (2008).
  - [24] S. S. Hodgman, R. G. Dall, K. G. H. Baldwin, and A. G. Truscott, Complete ground-state transition rates for the helium  $2^3P$  manifold, *Phys. Rev. A* **80**, 044501 (2009).
  - [25] B. M. Henson, X. Yue, S. S. Hodgman, D. K. Shin, L. A. Smirnov, E. A. Ostrovskaya, X. W. Guan, and A. G. Truscott, Bogoliubov-chenkov radiation in an atom laser, *Phys. Rev. A* **97**, 063601 (2018).
  - [26] I. Yavin, M. Weel, A. Andreyuk, and A. Kumarakrishnan, A calculation of the time-of-flight distribution of trapped atoms, *American Journal of Physics* **70**, 149 (2002).
  - [27] W. Whaling, P. Hannaford, R. Lowe, E. Biémont, and G. Nicolas, Absolute transition probabilities in vanadium I and the solar abundance of vanadium, *Astronomy and Astrophysics* **153**, 109 (1985).
  - [28] J. Pickering, R. Blackwell-Whitehead, A. Thorne, M. Ruffoni, and C. Holmes, Laboratory measurements of oscillator strengths and their astrophysical applications, *Canadian Journal of Physics* **89**, 387 (2011).
  - [29] X. Zheng, Y. R. Sun, J.-J. Chen, W. Jiang, K. Pachucki, and S.-M. Hu, Measurement of the frequency of the  $2^3S - 2^3P$  transition of  $^4\text{He}$ , *Phys. Rev. Lett.* **119**, 263002 (2017).
  - [30] C. J. Campbell, A. G. Radnaev, A. Kuzmich, V. A. Dzuba, V. V. Flambaum, and A. Derevianko, Single-ion nuclear clock for metrology at the 19th decimal place, *Phys. Rev. Lett.* **108**, 120802 (2012).
  - [31] L. von der Wense, B. Seiferle, M. Laatiaoui, J. B. Neumayr, H.-J. Maier, H.-F. Wirth, C. Mokry, J. Runke, K. Eberhardt, C. E. Düllmann, N. G. Trautmann, and P. G. Thirolf, Direct detection of the  $^{229}\text{Th}$  nuclear clock transition, *Nature* **533**, 47 (2016).
  - [32] L. von der Wense, B. Seiferle, and P. G. Thirolf, Towards a  $^{229}\text{Th}$ -based nuclear clock, *Measurement Techniques* **60**, 1178 (2018).
  - [33] B. Seiferle, L. von der Wense, P. V. Bilous, I. Amersdorfer, C. Lemell, F. Libisch, S. Stellmer, T. Schumm, C. E. Düllmann, A. Pálffy, and P. G. Thirolf, Energy of the  $^{229}\text{Th}$  nuclear clock transition, *Nature* **573**, 243 (2019).
  - [34] C. E. Tanner and C. Wieman, Precision measurement of the hyperfine structure of the  $^{133}\text{Cs}\ 6P_{3/2}$  state, *Phys. Rev. A* **38**, 1616 (1988).
  - [35] *Technical Information wavelengthmeter WS8-2*, HighFinesse GmbH (2019).
  - [36] D. A. Kondratjev, I. L. Beigman, and L. A. Vainshtein,

- Static polarizabilities of helium and alkali atoms, and their isoelectronic ions, *Journal of Russian Laser Research* **31**, 294 (2010).
- [37] P. S. Julienne and F. H. Mies, Collisions of ultracold trapped atoms, *J. Opt. Soc. Am. B* **6**, 2257 (1989).
- [38] T. C. Killian, D. G. Fried, L. Willmann, D. Landhuis, S. C. Moss, T. J. Greytak, and D. Kleppner, Cold collision frequency shift of the  $1S$ - $2S$  transition in hydrogen, *Phys. Rev. Lett.* **81**, 3807 (1998).
- [39] S. Moal, M. Portier, J. Kim, J. Dugué, U. D. Rapol, M. Leduc, and C. Cohen-Tannoudji, Accurate determination of the scattering length of metastable helium atoms using dark resonances between atoms and exotic molecules, *Phys. Rev. Lett.* **96**, 023203 (2006).
- [40] G. A. Pitz, D. E. Wertepny, and G. P. Perram, Pressure broadening and shift of the cesium  $D_1$  transition by the noble gases and  $N_2$ ,  $H_2$ ,  $HD$ ,  $D_2$ ,  $CH_4$ ,  $C_2H_6$ ,  $CF_4$ , and  $^3He$ , *Phys. Rev. A* **80**, 062718 (2009).
- [41] G. A. Pitz, C. D. Fox, and G. P. Perram, Pressure broadening and shift of the cesium  $D_2$  transition by the noble gases and  $N_2$ ,  $H_2$ ,  $HD$ ,  $D_2$ ,  $CH_4$ ,  $C_2H_6$ ,  $CF_4$ , and  $^3He$  with comparison to the  $D_1$  transition, *Phys. Rev. A* **82**, 042502 (2010).
- [42] J. L. Margrave, Vapour pressure of the chemical elements (Nesmeyanov, A. N.), *Journal of Chemical Education* **41**, A590 (1964).
- [43] A. Kramida, Y. Ralchenko, J. Reader, and NIST ASD Team, (2019), NIST Atomic Spectra Database (ver. 5.7.1), [Online]. Available: <https://physics.nist.gov/asd> [2019, November 10]. National Institute of Standards and Technology, Gaithersburg, MD.
- [44] J. Olivero and R. Longbothum, Empirical fits to the Voigt line width: A brief review, *Journal of Quantitative Spectroscopy and Radiative Transfer* **17**, 233 (1977).
- [45] M. C. E. Huber and R. J. Sandeman, The measurement of oscillator strengths, *Reports on Progress in Physics* **49**, 397 (1986).
- [46] M. Ligare, Classical thermodynamics of particles in harmonic traps, *American Journal of Physics* **78**, 815 (2010).
- [47] V. Krainov and B. M. Smirnov, Atomic and molecular radiative processes (Springer International Publishing, 2019) Chap. 1.2.4, pp. 26–30.
- [48] H. J. Metcalf and P. Van der Straten, Laser cooling and trapping (Springer-Verlag, New York, 1999) Chap. 4, pp. 53–56.

## Supporting Online Material

### Experimental Details

**Apparatus:** The laser used was an M squared SolsTiS, a widely tuneable (700 to 1000 nm) Ti:Sapphire laser, with an M squared ECD-X doubling cavity (providing light in a 350 to 500 nm range). The laser was stabilised at a specific frequency via a proportional-integral-derivative (PID) feedback loop between a HighFinesse/Ångstrom WS8-2 wavemeter, measuring the laser’s output, and the lab computer which controlled the scanning cavity within the SolsTiS. The power of the probe beam was measured just before the experimental chamber over time via the use of a photodiode, in order to calibrate the final signal with respect to incident power.

**Calibration of the Wavemeter:** The wavemeter was periodically calibrated by using saturated absorption

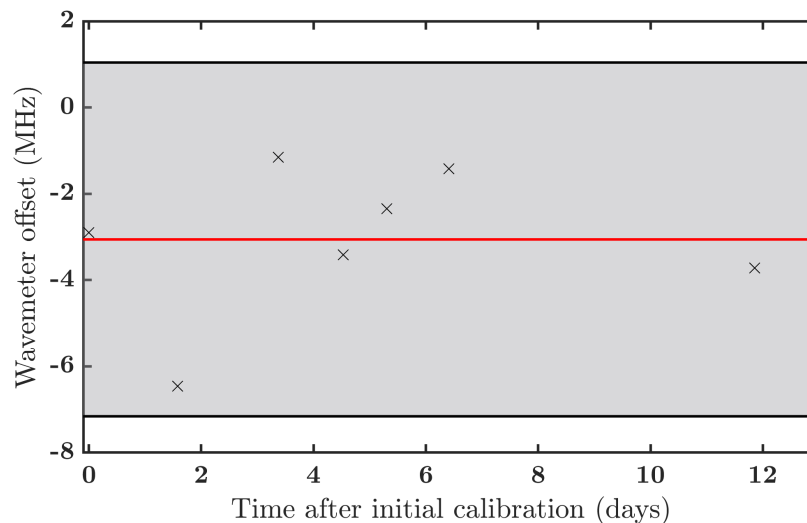


FIG. 5. Measured wavemeter offset versus time. Black x’s mark empirical data, with the red line showing the mean of the data  $-3.01$  MHz, and the black lines and shaded region indicating an uncertainty of  $4.1$  MHz, which arises from the specified manufacture error and the distribution of the data.



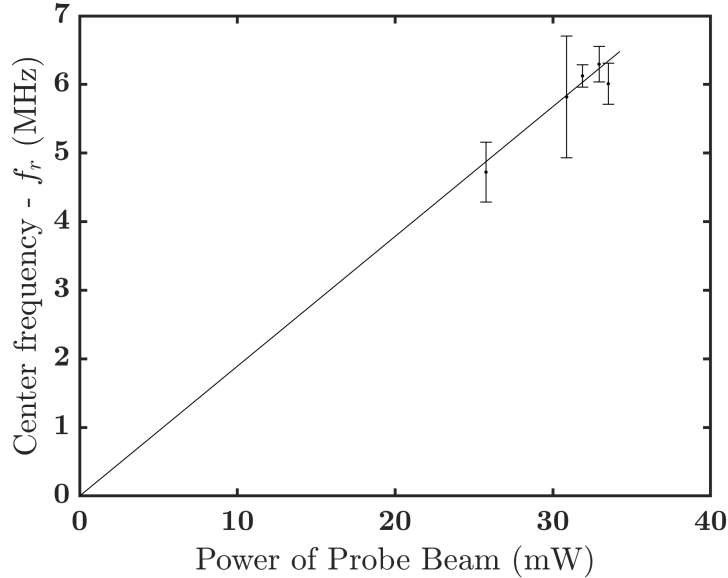


FIG. 6. Frequency center of the distribution relative to field free value  $f_r$  as a function of applied probe beam power.

spectroscopy in a cell with the non-doubled light (700 to 1000 nm) to perform measurement of a known cesium crossover transition from  $6^2S_{1/2}, F = 4$  to between  $6^2P_{3/2}, F = 4$  and  $6^2P_{3/2}, F = 5$ . This reference transition was constrained to be 351, 721, 835.0(1) MHz, equivalently 852.3566870(3) nm, by the measurement of Tanner and Wieman [34]. The reason this particular transition was chosen as a reference was that after applying the doubling cavity the light from this transition is  $\sim 1.5$  nm below the theoretically expected and experimentally measured wavelength of the transition of interest. From the manufacturer specifications we know that a calibration within 2.0 nm gives the wavemeter an accuracy of 2.0 MHz [35], however, as we are calibrating before the doubling cavity we must double this error to 4.0 MHz. The calibration shift in the wavemeter over time is shown in Fig. 5. We correct for systematic wavemeter drift using the average of the calibrations, a shift of  $-3.01$  MHz. The standard error in the distribution of the measurements was added to the fundamental wavemeter uncertainty to obtain a final uncertainty in this shift of 4.1 MHz.

**Detection:** The atoms are imaged in the far-field with full three dimensional resolution using an 80 mm diameter micro-channel plate and delay line detector located  $\sim 850$  mm below trap centre, with a spatial resolution of  $\sim 120 \mu\text{m}$  and temporal resolution of  $\sim 3 \mu\text{s}$  [21].

**Trap:** We use a magnetic bi-planar quadrupole Ioffe trap [20], which has trapping frequencies  $\omega_{(x,y,z)}/2\pi = (53.5(6), 426.56(5), 430.30(6))$  Hz. The trap frequencies of the magnetic trap were determined by inducing oscillations in the trap and then outcoupling portions of the atoms with RF pulses over time. From the measured 3D oscillations of the atoms we extract the trap frequencies.

**Alignment of the Probe Beam:** We also use our trap frequency measurement technique as a tool to align the probe beam. We looked for a difference in the trap frequency between when the probe beam was and was not applied to the atoms. This frequency change is due to the dynamic polarizability the probe beam exerts on the atoms, adding an additional trapping potential that is approximately harmonic, which in turn purely depends upon the wavelength and the intensity of the light applied. Hence by keeping the wavelength fixed we were able to maximize the alignment on the atoms via maximizing the change in trap frequency.

**Fundamental light:** To ensure we are not observing a two photon process caused by the non-doubled fundamental light of the laser we use a range of measures: there is a filter which blocks wavelengths around the fundamental range just before the optic fiber that directs the light to the experimental chamber; the laser table and experimental chamber are completely isolated from each other; and we observe linear scaling of the signal amplitude with power in agreement with a single photon process.

### Systematic Frequency Shifts

**Zeeman shift:** The transition frequency is shifted by the Zeeman effect due to the energies of the initial and final states being shifted by different amounts due to external magnetic fields. The magnitude of the external field at the atoms is measured to be approximately 0.613(1) G, by using a swept RF pulse to measure the Zeeman splitting between the  $2^3S_1$ ,  $m_J = +1$  and  $m_J = 0$  states. Note the magnitude of the magnetic field does not change between the direct detection and heating method. At field strengths of this size only the linear Zeeman effects will be relevant to our experimental precision. The frequency shift due to the linear Zeeman effect has the functional form

$$\Delta f = \frac{\mu_B}{h} B(m_{J,e}g_{j,e} - m_{J,g}g_{j,g}), \quad (1)$$

where  $\mu_B$  is the Bohr magneton,  $h$  is the Planck constant,  $B$  is the magnetic field magnitude,  $g_{j,e}$  and  $g_{j,g}$  are the Landé  $g$ -factors of the excited and ground states respectively, and  $m_J$  are their respective magnetic quantum numbers. The atoms are initially in the  $2^3S_1$ ,  $m_J = +1$  state with  $g_j = 2.0$  and are excited to the  $3^3S_1$ ,  $m_J = 0$  state with  $g_j = 2.0$ . Hence the Zeeman shift for our transition is  $\Delta f_{Zeeman} = -1.715(3)$  MHz.

**AC Stark shift:** For the tested experimental range the AC Stark shift is linearly proportional to the intensity of the probe beam at the atoms. Note we do not use any other light source in our trapping potential. As the focus of the probe beam is kept constant, the AC stark shift is linearly dependant on the total power in the beam. The power of the probe beam was measured using a calibrated photodiode. The frequency of the transitions was measured at a range of probe beam powers, as shown in Fig. 6. The data can then be used to linearly extrapolate to a field-free value of the frequency, with an uncertainty determined by the confidence interval of the fit. For the direct detection method we find a shift of  $\Delta f_{AC,Probe} = 8.6(1.5)$  MHz and for the heating method  $\Delta f_{AC,Probe} = 5.9(1.6)$  MHz. The reason these values differ is the applied probe beam's focus size varied between the methods.

**DC Stark shift:** For a multi-electron atom in either ground or low excited state in the presence of a weak static electric field its energy levels will be shifted as  $\Delta E = -\frac{1}{2}\alpha_s \mathbf{E}_{dc}^2$ , where  $\alpha_s$  is the static polarisability of the atoms (in their current state) and  $\mathbf{E}_{dc}$  is the dc electric field of strength. As the electric field is kept constant the shift in frequency due to this effect is given by  $\Delta f_{DC} = -\frac{1}{2h}\Delta\alpha_s \mathbf{E}_{dc}^2$ . For our case we can constrain from direct measurement that any static electric field in our experimental chamber has  $\mathbf{E}_{dc} < 2$  kV/m and  $\Delta\alpha < 6 \times 10^{-50}$  C<sup>3</sup>m<sup>3</sup>/J<sup>2</sup> [36], thus  $\Delta f_{DC} < 10^{-10}$  Hz.

**Mean field shift:** The interactions between atoms in a BEC can also shift spectral lines, termed the mean field shift. For bosonic particles with sufficiently low temperatures such that only  $s$ -wave scattering will occur, which for the case of He\* corresponds to temperatures less than 100 mK [37], the density dependent mean field shift of the atomic energy level in a degenerate homogeneous system is given by [38]

$$\Delta E = \frac{8\pi\hbar^2 a n}{m}, \quad (2)$$

where  $a$  is the scattering length of the atoms in their current state,  $m$  is the mass of the atoms and  $n$  is the density of the atoms. The frequency shift induced in the spectroscopic transitions is hence  $\Delta f_{mf} = \frac{4\hbar}{m}(n_f a_f - n_i a_i)$ , where  $a_i$  and  $a_f$ , and  $n_i$  and  $n_f$  are the scattering length and density of the atoms in the initial and final states respectively. As the transition we are considering is extremely weak the density of the final state would be negligible, and thus  $\Delta f_{mf} \approx -\frac{4\hbar}{m}n_i a_i$ . The scattering length of the  $2^3S_1$  state is of the order of 10 nm [39] and the average density of the atoms can be calculated from the atom number and the trap frequencies to be on the order of  $10^{19}$  m<sup>-3</sup>. This gives us a mean field shift of the order  $\Delta f_{mf} \sim 10$  kHz.

**Recoil shift:** Due to the conservation of momentum, when a photon is absorbed during an atomic transition the photon's momentum is imparted onto the atom. The momentum of the photon, and thus the change in momentum of the atom, is given by  $\Delta p = \frac{\hbar f}{c}$ , where  $f$  is the frequency of the absorbed photon and  $c$  is the speed of light. This increase in the kinetic energy of the atom must come from the photon, implying that there must be a shift in the energy of the photon in order to compensate for this imparted energy. The recoil shift of the photon's energy is  $\Delta E = \frac{1}{2m} \left(\frac{\hbar f}{c}\right)^2$ , where  $m$  is the atomic mass. The frequency of the transition was measured to be 700,939,270(5) MHz giving a recoil shift of 0.273 MHz. As the relative uncertainty is on the order of parts per hundred-million the uncertainty within the recoil shift is well below 1 kHz.



**Cesium Cell offset:** There are two main systematic shifts which occur in the cesium cell used to spectroscopically reference the wavemeter and laser: the AC Stark shift due to the probe laser and the vapour (or pressure) shift due to collisions within the cell. The AC Stark shift can be determined in the same manner as it was for the probe beam, by varying the power and measuring the change in the center frequency and then extrapolating to a theory free value, see Fig. 7. The normal applied laser power is 560  $\mu\text{W}$  which gives an AC stark shift of  $\Delta f_{AC,Cs} = -1.9(4)$  MHz. The pressure shift in the cell can be constrained using literature values, which state that the pressure shift is less than 30 MHz/torr [40, 41]. The cell was at a temperature of 84(1)  $^{\circ}\text{C}$  which corresponds to a vapour pressure of  $2.00(2) \times 10^{-4}$  torr [42]. Thus the vapour pressure shift in the cell is constrained to be  $\Delta f_{pressure} < 6 \times 10^{-3}$  MHz.

### Details of Heating Method

Fig. 8a displays the number of counts detected versus time, with a broadened radio frequency pulse applied to the trapped atoms every 240 ms corresponding to the peaks present in the profile. If we zoom in on a particular peak (Fig. 8b) we can see it has a distinctive Gaussian profile. From Yavin *et al.* [26] we know that the expected time of flight probability density profile for a ballistic expansion of particles from a point source is

$$n(t) = A\pi v_0^2 \left( \frac{\frac{1}{2}gt^2 + d}{t^2} \right) \exp \left( -\frac{(\frac{1}{2}gt^2 - d)^2}{v_0^2 t^2} \right), \quad (3)$$

where  $d$  is the fall distance from the trap to the detector,  $A = (m/2\pi k_B T)^{3/2}$ ,  $m$  is the mass of a particle,  $k_B$  is the Boltzmann constant,  $v_0 = \sqrt{2k_B T/m}$  is the most probable velocity, and  $g = -9.81 \text{ m/s}^2$  is the acceleration due to gravity. If the spread of the peak is small in time we can simplify Eqn. 4 by approximating it as a Gaussian

$$n(t) \approx A\pi v_0^2 \left( \frac{1}{2}g + \frac{d}{t_f^2} \right) \exp \left( -\frac{(t - t_f)^2}{2 \left( \frac{2}{g} \sqrt{\frac{k_B T}{m}} \right)^2} \right), \quad (4)$$

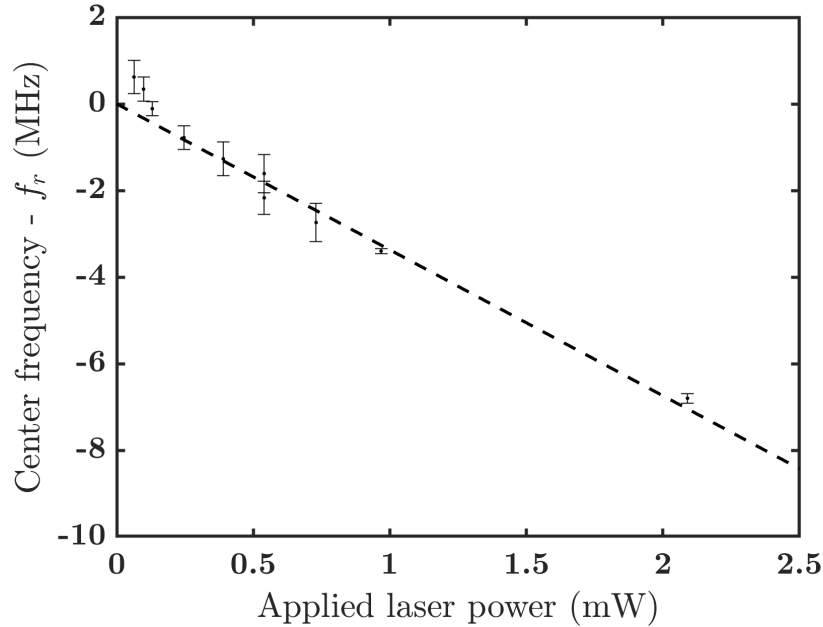


FIG. 7. Measured center frequency of cesium calibration transition relative to the extrapolated theory free value  $f_r$  as a function of applied laser power. The dashed line represents linear best fit, with equation  $f_{rel} = -3.37 \times 10^{-3} P$  where  $f_{rel}$  is the relative frequency in MHz and  $P$  is the applied power in  $\mu\text{W}$ .

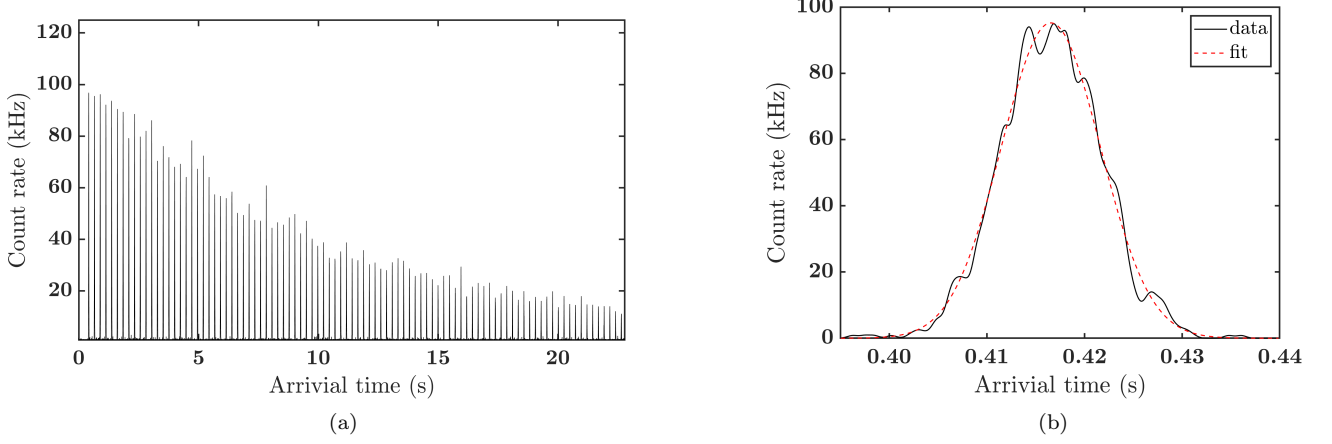


FIG. 8. (a) Time of flight profile for the heating method consisting of 95 outcoupled atomic pulses. The outcoupled atoms arrive at the detector in pulses, signified by the peaked structure of the profile. Arrival time is measured from when the first outcoupling pulse is applied. (b) Zoom in of the first pulse, with the solid black line representing count rate over time and the dashed red line indicating a Gaussian fit. This particular fit has parameters  $t_0 = 1.756(1)$  s,  $\sigma_t = 0.0051(1)$  s (equivalent to  $T = 1.21(2)$   $\mu$ K), and  $C_0 = 96(2)$  kHz.

where  $t_f = \sqrt{\frac{2d}{g}}$  is the expected fall time for particles with zero velocity. Thus we fit a Gaussian to the count rate distribution in time  $C(t)$  of the form,

$$C(t) = C_0 e^{-\frac{(t-t_0)^2}{2\sigma_t^2}}, \quad (5)$$

where  $C_0$  is the peak count rate,  $t_0$  is the center time of the distribution (the time of arrival for particles with zero initial vertical velocity), and  $\sigma_t$  is the standard deviation. From Eqn. 4 we have  $\sigma_t = \frac{2}{g} \sqrt{\frac{k_B T}{m}}$ . Rearranging we obtain,

$$T = (-g\sigma_t/2)^2 \times \frac{m_{He}}{k_B} \quad (6)$$

From the fits of each pulse we extract the temperature versus time (see Fig. 9) and fit a line to this data, the gradient of which gives us the heating rate. The comparison of the heating rate with the probe applied to a reference then gives us a measure of the temperature increase purely due to photon absorption.

### Theoretical Value of the excited state lifetime of the $3^3S_1$ state in helium

The excited state lifetime is the average amount of time an atom will remain in a particular excited state before decaying to a lower energy state. The state lifetime  $\tau_u$  can be calculated for a given state  $u$  from the Einstein  $A$  coefficients of all transitions to lower lying states,

$$\tau_u = \frac{1}{\sum_l A_{ul}}, \quad (7)$$

where  $A_{ul}$  denotes the Einstein  $A$  coefficient for the transition between the upper  $u$  and the lower state  $l$ . For the  $3^3S_1$  state of helium the major contributions to the state lifetime are from the transitions to the  $2^3P_{0,1,2}$  states, which have respective Einstein  $A$  coefficients  $J = 0$   $A = 3.095(9) \times 10^6$  s $^{-1}$ ,  $J = 1$   $A = 9.28(3) \times 10^6$  s $^{-1}$ , and  $J = 2$   $A = 1.55(5) \times 10^7$  s $^{-1}$  [43]. Hence the theoretically expected state lifetime of the  $3^3S_1$  state is  $\tau = 35.9(2)$  ns.

### Experimental determination of Excited state lifetime

The scattering probability distribution in frequency space of an individual transition forms a Lorentzian distribution, whose linewidth, or more precisely full width half maximum (FWHM),  $\Gamma$  is related to the state lifetime of the excited

state of the transition  $\tau$  by  $\tau = 1/(2\pi\Gamma)$ . However, the experimentally measured values of the absorption linewidth,  $\Gamma_d = 5.74(28)$  MHz and  $\Gamma_h = 5(1)$  MHz (see Fig. 3 and Fig. 4 respectively in main text), is broadened by a number of factors; primarily our effective laser linewidth, and the mean field broadening, whose FWHM we denote  $\Gamma_l$ , and  $\Gamma_{mf}$  respectively.

The effective laser line width was measured by taking the standard deviation of the calibration data, see Fig. 5, which can be converted to a FWHM assuming the distribution is Gaussian by multiplying by  $2\sqrt{2\ln(2)}$  giving  $\Gamma_l = 1.9(7)$  MHz, where the error is calculated from the standard error of the sample standard deviation of normally distributed data. An approximate value for the mean field broadening can be obtained from the mean field shift calculated above, hence for both methods we have  $\sigma_{mf} \sim 0.01$  MHz, which converted to a FWHM is  $\Gamma_{mf} \sim 0.024$  MHz.

The broadening effects have Gaussian distributions, and hence when they convolve with our signal which has a Lorentzian distribution they form a Voigt distribution. Note that we fit a Lorentzian to our data rather than a Voigt function for technical ease, due to the broadening effects being small in comparison to the width of the signal, and hence the Lorentzian fit gives a reasonably accurate measure of the FWHM of the true Voigt distribution. The FWHM of a Voigt distribution is given approximately by  $\Gamma_V \approx 0.5346\Gamma_L + \sqrt{0.2166\Gamma_L^2 + \Gamma_G^2}$  [44] where  $\Gamma_L$  and  $\Gamma_G$  are the FWHM's of the Lorentzian and Gaussian distributions being convolved. For the direct detection method we have  $\Gamma_V = 5.74(28)$  MHz and as the mean field contribution is negligible compare to the laser linewidth the broadening sources can be considered one Gaussian with FWHM  $\Gamma_G = 1.9(7)$  MHz. Inverting this relationship we obtain the FWHM of the true distribution  $\Gamma_L = 5.0^{+0.6}_{-1.0}$  MHz, which gives us our excited state lifetime of  $\tau = 33(6)$  ns for the direct detection method. Following the same method for the heating method, with values  $\Gamma_V = 5(1)$  MHz and  $\Gamma_G = 1.9(7)$  MHz, we obtain  $\Gamma_L = 4.2^{+1.5}_{-2.0}$  MHz and hence  $\tau = 40(20)$  ns.

### Experimental determination of Einstein $A$ coefficient

In this section we present a derivation of an expression for the Einstein  $A$  coefficient that is entirely dependant on empirical data and known quantities, starting from a fundamental expression, Eqn. 8. First consider light with frequency  $f$  and intensity distribution  $I_f(x, y, z)$  propagating along the  $x$ -axis through some absorbent medium. The change in intensity at a particular point  $\delta I_f(x, y, z)$  over a small distance  $\delta x$  is given by the expression [45]

$$-\delta I_f(x, y, z) = k(f, x, y, z) I_f(x, y, z) \delta x, \quad (8)$$

where  $k(f, x, y, z)$  is the frequency and density dependant absorption coefficient. Let the total power in the light field at point  $x$  be  $P_f(x)$  and  $I_f(x, y, z) = P_f(x)\phi_I(x, y, z)$ , where  $\phi_I(x, y, z)$  is a function that gives the distribution of the power over a given plane and has unit normalisation. We can hence integrate Eqn. 8 over the  $y$ - $z$  plane, the

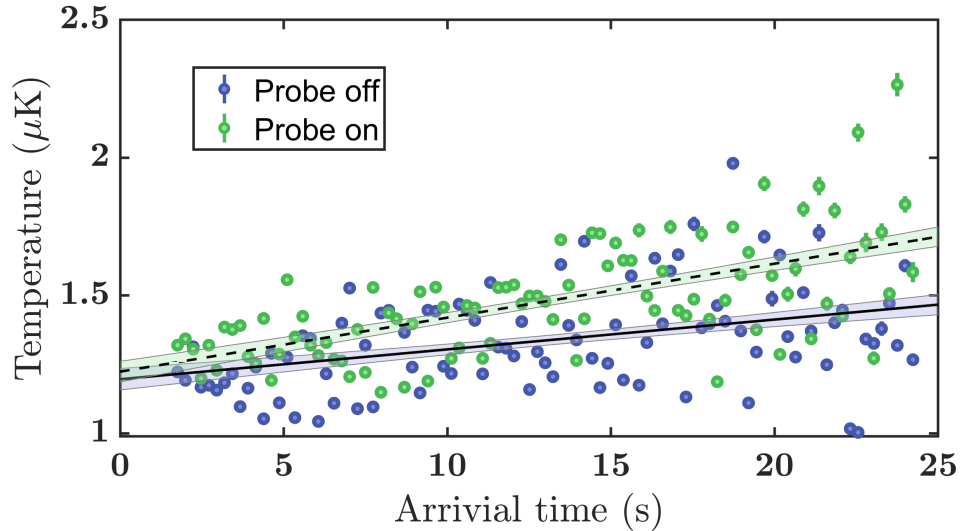


FIG. 9. Measured temperature versus arrival time for a particular run of the heating method with the probe beam applied (dashed green) and the probe beam blocked as a reference (solid blue). Each individual point on the plot corresponds to an individual pulse, see Fig. 8a and Fig. 8b.

plane perpendicular to the direction of light propagation, and obtain the change in power  $\delta P_f(x)$  over an infinitesimal distance  $\delta x$  is

$$-\delta P_f(x) = P_f(x) \delta x \int \int dy dz k(f, x, y, z) \phi_I(x, y, z) \quad (9)$$

$$\therefore -\frac{\delta P_f(x)}{P_f(x)} = \delta x \int \int dy dz k(f, x, y, z) \phi_I(x, y, z). \quad (10)$$

Both sides of Eqn. 10 can be integrated to obtain,

$$-\int \frac{dP_f(x)}{P_f(x)} = \int \int \int dx dy dz k(f, x, y, z) \phi_I(x, y, z) \quad (11)$$

$$-\log \left( \frac{P_f^+}{P_f^-} \right) = \iiint_{all\ space} k(f, x, y, z) \phi_I(x, y, z), \quad (12)$$

where  $P_f^-$  is the power in the light field before moving through the medium, in a theoretical sense the power at  $x = -\infty$ , and  $P_f^+$  is the power in the light field after the medium, *i.e.* the power at  $x = +\infty$ . Next we note that the integral of the absorption coefficient over the line shape of a transition is related to the Einstein  $A$  coefficient as follows [45]:

$$\int_{line} k(f, x, y, z) df = \frac{c^2}{8\pi f_0^2} A_{ul} n(x, y, z), \quad (13)$$

where  $f_0$  is the center frequency of the transition,  $A_{ul}$  is the Einstein  $A$  coefficient for the transition between the states  $u$  and  $l$ , and  $n(x, y, z)$  is the atomic density distribution at the point  $(x, y, z)$ . Therefore Eqn. 12 can be written as

$$-\int df \log \left( \frac{P_f^+}{P_f^-} \right) = \iiint_{all\ space} \frac{c^2}{8\pi f_0^2} A_{ul} n(x, y, z) \phi_I(x, y, z), \quad (14)$$

where we have assumed the intensity distribution is frequency independent. To simplify Eqn. 14 further, we assume that the power removed from the beam is small and so we can Taylor expand  $-\log \left( \frac{P_f^+}{P_f^-} \right)$  about 1 as  $-\log \left( \frac{P_f^+}{P_f^-} \right) \approx \frac{P_f^- - P_f^+}{P_f^-}$ . The difference between the initial and final powers is equal to the rate of photons scattered by the atoms multiplied by the energy of the photon,  $P_f^- - P_f^+ = hf \frac{dN_{scatter}}{dt}$ . The number of scattered photons can be calculated from the frequency dependant heating rate due to the probe beam  $\frac{dT}{dt}(f)$ , the heat capacity of the atoms, which for a thermal gas in a constant harmonic trap is  $C_b = 3Nk_B$  [46], and the average energy added to the gas by each photon  $E_p$ , from the relation  $\frac{dN_{scatter}}{dt} = \frac{dT}{dt}(f) \frac{C_b}{E_p}$ . We can simplify even further by utilising the relation  $n(x, y, z) = N\phi_N(x, y, z)$ , where  $N$  is the total atom number and  $\phi_N(x, y, z)$  gives the atomic density distribution with unit normalisation. Combining we see Eqn. 14 becomes,

$$\int df \frac{hf}{P_f^-} \frac{dT}{dt}(f) \frac{C_b}{E_p} = \frac{c^2}{8\pi f_0^2} A_{ul} \iiint_{all\ space} \phi_N(x, y, z) \phi_I(x, y, z) \quad (15)$$

$$\therefore A_{ul} = \frac{24\pi f_0^2 h k_B}{c^2 E_p} \frac{\int df f \left( P_f^- \right)^{-1} \frac{dT}{dt}(f)}{\iiint_{all\ space} \phi_N(x, y, z) \phi_I(x, y, z)}. \quad (16)$$

The parameters in Eqn. 16 are all experimentally measured or determined as follows:  $f$  is measured by the HighFinness wavemeter,  $P_f^-$  is measured by a calibrated photodiode,  $\frac{dT}{dt}$  is extracted from the data as described in the heating method section,  $\phi_I(x, y, z)$  is measured via a camera,  $\phi_N(x, y, z)$  can be determined by the trapping frequency and temperature [46],  $E_p = \frac{1}{2m} \left( \frac{hf_0}{c} \right)^2$  is given by the recoil momentum of the photons, and the remaining parameters are all known constants.

$^3S_1$	$^3P_J$									
$m_J$	J $m_J$	0	1			2				
		0	+1	0	-1	+2	+1	0	-1	-2
+1		2	3	3	-	6	3	1	-	-
0		2	3	0	3	-	3	4	3	-
-1		2	-	3	3	-	-	1	3	6

TABLE III. Transition strengths in the D-line of He\* obtained from the mod square of the Clebsch-Gordan coefficient and normalised to the weakest allowed transition [48]. To obtain fractional transition rates divide the values in the relevant row or column by its respective total (18 for rows and 6 for columns).

### Clebsch-Gordan coefficients

The Clebsch-Gordan coefficients represent the angular momentum coupling between different atomic states. For our work they are relevant because the modulus squared of the Clebsch-Gordan coefficient between two particular magnetic substates is equal to the relative intensity, or probability, of that transition in comparison to all other transitions between the two respective manifolds [47]. The relative transition strengths, normalised to the weakest allowed transition, between the  $^3S_1$  and  $^3P_{0,1,2}$  manifolds are given in Tab. III [48]. Given that the excited particle is initially in the  $^3S_1$ ,  $m_J = 0$  state and the transitions from this state are dominated by decays to the  $2^3P_{0,1,2}$  states, and then from those states the transitions are dominantly towards the  $2^3S_1$  state, we can calculate the probability of an atom decaying to each magnetic sub state from Tab. III. The initial relative transition probabilities from the  $^3S_1$ ,  $m_J = 0$  state are given by the second row of Tab. III, and the exact fraction can be obtained by normalising the row by its sum 18. The transitions from the  $2^3P_{0,1,2}$  magnetic sub states to the  $2^3S_1$ ,  $m_J = (+1, 0, -1)$  sub states are given by the column of each relevant state (specifically all states except  $2^3P_2$ ,  $m_J = \pm 2$  as  $m_J$  can at most change by one), and again the fractions can be obtained by normalising each column by its total 6. From this we obtain the fraction of atoms that decay down each of the possible paths, and after summing the fractions which lead to each final state we obtain the total fraction that end up in each  $2^3S_1$ ,  $m_J = (+1, 0, -1)$  state as  $(\frac{26}{108}, \frac{56}{108}, \frac{26}{108})$  or as approximate percentages (24%, 52%, 24%).

### RF Knife

For the direction detection method a constant radio frequency field was applied to the atoms during the detection phase. The reason for this was to attempt to increase the detection efficiency of atoms which absorb a photon by both outcoupling some portion of atoms which decay back to the trapped  $2^3S_1$ ,  $m_J = +1$  state, and lensing these atoms so that a higher proportion would land on the detector.

Consider that the two subsequent photon decays produce a momentum distribution which is a filled shell with a center translated by an outer radius equal to a 427 nm photon recoil. As the maximum magnetic field experienced by an atom oscillating in the magnetic trap is proportional to its maximum kinetic energy, by applying RF radiation tuned to the  $2^3S_1$ ,  $m_J = 1 \rightarrow 0$  transition for a given magnetic field strength we can selectively outcouple atoms with maximum kinetic energy above a threshold. Furthermore, as the trap does work on an atom the momentum space distribution of these outcoupled atoms is reduced in size, hence improving collection efficiency. Thus while only  $\sim 24\%$  of atoms decay to the  $2^3S_1$ ,  $m_J = +1$  state via this process they could theoretically significantly increase the total signal amplitude. The interplay between these two effects produce an optimum collection efficiency that depends on the particular momentum distribution and detector geometry.

It was found experimentally, however, that there was no statistically significant increase in the signal amplitude between the RF field applied and not applied. The exact reasons for this are unknown but we conjecture that the rescattering rate and the RF not saturating the transition are the most likely contributing factors.

### Sensitivity Metric

The sensitivity metric which we quote is defined as the transitions with the smallest Einstein  $A$ ,  $A_{min}$ , that the given technique can detect for a given power, atom number and interrogation time. In order to understand how

this is calculated consider a technique which is used to measure a transition with Einstein  $A$  Coefficient  $A_0$ . If the technique produces a peak signal-to-noise ratio  $\sigma_{max}$  after interrogating  $N$  atoms for a total time  $t$  with power  $P$ , from Poissionian statistics we can see that the signal-to-noise ratio should scale approximately as  $\sigma(N, t, P) \approx \frac{\sigma_{max}}{\sqrt{NtP}}$ . Next we make the assumption that in order to detect a transition we require a signal to noise ratio of  $\sim 2 : 1$ . Hence if our signal scales linearly with  $A_0$  we have

$$A_{min}(N, t, P) = \frac{2A_0}{\sigma(N, t, P)}. \quad (17)$$

For the direct detection method we have  $\sigma_{max} = 25.96$  for  $N = 1.7 \times 10^6$  atoms,  $t = 25 \times 215$  s (as we interrogate for 25 s for each of the total of 215 measurement shots), and  $P = 26$  mW. Thus  $A_{min} = 5 \times 10^{-10}$  s<sup>-1</sup> and  $A_{min}(N, t, P) = 8.3 \times 10^{-6}$  s<sup>-1</sup>√atom J. For the heating method  $\sigma_{max} = 7.83$  for  $N = 1 \times 10^7$  atoms,  $t = 25 \times 188$  s, and  $P = 17.8$  mW, thus  $A_{min}(N, t, P) = 5.2 \times 10^{-5}$  s<sup>-1</sup>√atom J and  $A_{min} = 1.79 \times 10^{-9}$  s<sup>-1</sup>.